SYMPOSIUM ON SIMULATION IN ARCHITECTURE + URBAN DESIGN
SimAUD 2020

Hydrogel-Based Evaporative and Radiative Cooling Prototype for Hot-Arid Climates

Dorit Aviv[12], Maryam Moradnejad[3], Aletheia Ida[3], Zherui Wang[1], Eric Teitelbaum[1], Forrest Meggers[1]

[1]Princeton University
Princeton, NJ, USA
dorit@princeton.edu

[2]Univeristy of Pennsylvania
Philadelphia, PA, USA

[3]University of Arizona
Tucson, AZ,USA

ABSTRACT

A roof aperture lined with hydrogel membrane is proposed for combined evaporative and radiative cooling in the desert climate. In order to determine the design, materials and predicted performance of this device, several types of digital simulations and physical experiments were performed. The proposed full-scale prototype, planned to be built and tested in Tucson, Arizona, responds to the climate's extreme diurnal temperature gradient through the use of adaptive materials. During the day, the roof aperture acts as a downdraft chimney, trapping the hot dry air passing through it. The funnel-shaped top of the chimney is embedded with a wet hydrogel membrane, which humidifies the air, causing instantaneous cooling and a consequent downdraft airflow into the building's interior. During the night, pockets of enclosed hydrogel encapsulated in the roof's structural frame are exposed to radiative cooling from the night sky and act as thermal storage for additional cooling during daytime. The complexity of the system requires several simulation and physical testing methods to be employed simultaneously: digital simulation tools of CFD, solar radiation analysis, radiative heat loss analysis were employed to analyze the overall geometry's effect on airflow radiant heat exchange; physical bench tests were conducted to analyze the performance of hydrogel membrane and compare it to other materials. A full-scale prototype will be built to validate the results of the model.

Author Keywords

Energy Performance; Airflow Simulation; Responsive Envelope; Material Properties; Hydrogel Membrane

ACM Classification Keywords

I.6.1 SIMULATION AND MODELING

1 INTRODUCTION

A roof aperture prototype channeling airflow into the building's interior is constructed in the Sonoran Desert of Tucson, Arizona in the Southwestern United States to take advantage of two cooling strategies enabled by the extreme dryness of the air in desert climates: evaporative cooling and radiant cooling (see Fig. 1).

First, evaporative cooling is highly effective in this climate because of the low dew point, allowing for significant air temperature drop per mass of water evaporated into the air. The system developed here takes advantage of a combination of evaporative cooling and thermal buoyancy force: the aperture acts as a downdraft chimney that evaporatively cools the air around the chimney's crown by exposing it to a wetted hydrogel membrane surface. The moisture causes the air to instantaneously cool and fall down the chimney into the building's interior volume due to gravity of the denser air mix. Several researchers have described the benefits of downdraft cooling in hot dry climates [1,2]. A downdraft system for the desert has also been exhaustively studied in the context of energy production at the infrastructure scale [3].

Second, the chimney's enclosure is constructed of high-heat-capacity materials in order to gain further passive cooling through radiant exchange with the sky. The low humidity and clear skies in Arizona allow for efficient longwave radiative heat exchange between the cold sky and the thermal mass stored in the roof structure. The challenge this second strategy presents in the context of the desert is the extremely high incident solar radiation that would be absorbed by the thermal mass and cause it to heat during the day far beyond the cooling exchange with the sky. A method to provide shading from direct solar radiation must be provided, while still allowing an optical exposure to the sky. Additionally, the thermal mass must be insulated from heat gain by the hot ambient air during the day.

One solution, proposed by Craig et al [4] suggests the use of roof insulation which provides a barrier for convective heat transfer while still allowing for longwave infrared radiation to infiltrate through it. Raman et al [5] achieved radiative cooling to nearly 5oC below the ambient air temperature under direct sunlight using a thermal photonic approach with a photonic solar reflector that reflects 97% of the incident sunlight while emitting strongly and selectively in the atmospheric transparency window. Ambient convective gains are prevented by an enclosed space between the exterior air and the panel's surface. Using the same strategy, Goldstein et al [6] demonstrate fluid cooling panels that harness radiative sky cooling to cool fluids

below the air temperature. Our approach is similar, as we insulate the thermal mass from ambient air with an infrared transparent membrane, while the interior temperature inside of the chimney is constantly lower than the exterior temperature due to the evaporatively induced downdraft airflow.

The thermodynamics and geometry optimization of a dual-function cooling roof chimney has been initially studied in previous work [7,8] . In this current prototype, we have developed a system which uses hydrogel membrane as the interface for the heat transfer between the exterior and interior environments. The hydrogel membrane acts both as thermal storage material for the building's envelope and as the interface layer through which water vapor is diffused into the air for evaporative cooling.

Hydrogel is a hydrophilic three-dimensional water-swollen polymer. The material chemistry consists of a range of compositions with two basic types: polyacrylamides and polysaccharides. Polyacrylamides are comprised of chemical covalent bonds providing strong and irreversible crosslinks for longevity and durability of the polymer. Polysaccharides are comprised of physical bonds, such as van der Waals forces, and result in weak crosslinks for reversibility and down-cycling of the polymer. Each has their advantages and can be optimized for different functionality with a range of environmental impacts. Some unique benefits of using hydrogel as a building material include the translucent optical properties to provide natural daylighting and the thermal capacitance when saturated with water. In addition, the hydrogel allows for diffusion of moisture for evaporative cooling processes in a passive mode: the moisture will evaporative from the surface area of the membrane based on vapor pressure differentials, thereby intelligently responding to low-humidity environments for passive cooling.

Prior applications of hydrogel in building material systems include the CloudGel glazing system invented by Charoudi for Saint Gobain [9] to provide dynamic natural daylighting and heat transfer control. Another more recent application in the building material market is the hydrogel-lined ceramic blocks from the IAAC group in Spain [10], which provides evaporative-cooling through modular natural ventilation apertures. Early membrane studies for evaporative-cooling with natural ventilation demonstrate the unique correlations between dynamic daylighting and heat transfer with varying saturation rates [11,12]. In these earlier studies, the swelling and deswelling kinetics of hydrogel membranes are considered for providing actuation of ventilation apertures and modulation of airflow and daylighting dynamics. Thermophysical properties of hydrogel diffusion kinetics are studied for other applications [13-16]. As of date, there are very limited implementations of hydrogel in building integration in part due to market constraints (emerging material translated from biotechnology applications), and in part due to limits on degradation cycling and fatigue (not yet demonstrated for building system applications). However, our work exposes the opportunities for multifunctional environmental response through ongoing research with these membranes.

2 METHODS

Due to the complexity of this dual-cooling system integrated into the proposed full-scale prototype (Fig. 1), multiple digital simulations and physical tests were conducted. The following sections will present various methods: first, bench-scale physical tests for the evaporative cooling capacity of the hydrogel membrane and the radiative cooling capacity of the thermal mass; then, digital simulations for the radiative exchanges and airflow dynamics of the full-scale prototype.

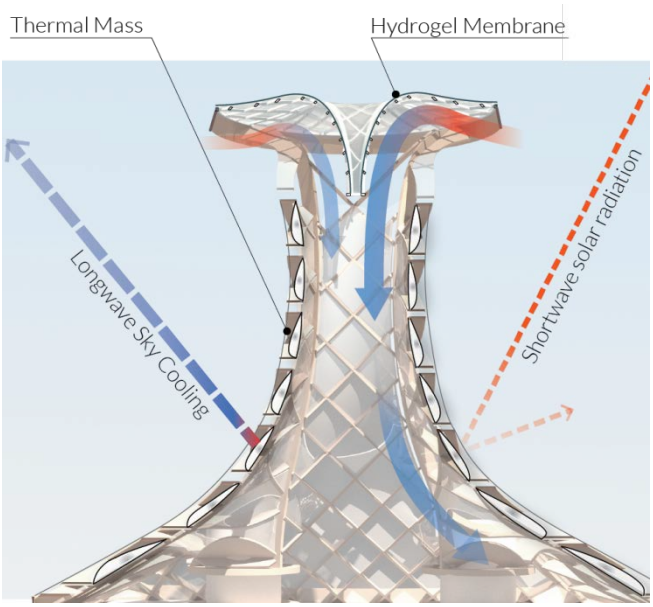

Figure 1. Diagram of the proposed prototype and its different cooling aspects to be simulated and tested: 1. the Hydrogel membrane's evaporative cooling capacity: once the hot dry air is humidified by water vapor diffusion from the hydrogel membrane embedded in the chimney's top funnel, it cools and drops down into the space below; 2. the thermal mass' radiative longwave sky cooling potential and shading/reflection of shortwave solar radiation through shortwave reflecting coating

2.1 Material Testing

2.1.1. Evaporative Cooling: Hydrogel

The evaporative cooling membrane is designed and engineered to accommodate effective diffusion and re-hydration in the large-scale surface area application for the downdraft chimney.

2.1.1.1. Diffusion Calculations

Diffusion of moisture from the hydrogel membrane is dependent on two major variables: hydrogel mesh pore size and vapor pressure differential with surrounding air. The mesh pore size of hydrogel is controlled through the ratio of crosslink monomers during synthesis as per the Flory-

Rehner theory: the greater concentration of crosslink monomer, the smaller the mesh pore size [17]. Because some structural integrity is needed for maximizing the exposed surface area of the diffusion membrane in this application, there is a balance that is needed between large pore size to accommodate optimal diffusion with small pore size to accommodate higher strength. The polyacrylamide gel synthesized for the current project is a 4% crosslink ratio. Upon full-scale physical prototype testing, the hydrogel synthesis will be modified to optimize diffusion and strength relationships in the membrane application.

The chemistry of the hydrogel also enables the ability for moisture diffusion. In this case, we synthesize a polyelectrolyte gel to enable more ease of release of the water molecules from the polymer chains. Future work may also incorporate chemistry modifications for optimized diffusion rates.

The vapor pressure differential is determined by the surrounding relative humidity (amount of moisture in the air as a ratio of the maximum amount that the air-mix could hold before saturation). The lower the relative humidity, the lower the vapor pressure in the surrounding air, which will enable higher rates of diffusion. Hotter air can hold more moisture, so typically consists of a lower relative humidity, which affords effective evaporative-cooling and diffusion rates. In our application, we assume a fully wetted surface of the hydrogel membrane and calculate based on an hourly rate as follows:

$$g_h = \theta_w A_w(x_s\text{-}x)$$

where g_h is the amount of water evaporated per hour, θ_w is the evaporation coefficient of water, A_w is the exposed wet surface area of the membrane, and x_s-x is the difference between the maximum humidity ratio and the actual humidity ratio of surrounding air (temperature-dependent) respectively. The evaporation coefficient for water is assumed at 0.5 based on comprehensive literature review on the subject [18-21].

We incorporate four daily peak relative humidity (RH%) and dry-bulb temperature (DBT) conditions for annual calculations on vapor diffusion potential. The TMYIII climate data for Tucson, Arizona provides the following peak DBT and RH% values:

March 21st (03.21):	24.2 °C 10% RH
June 21st (06.21):	37.2 °C 19% RH
September 21st (09.21):	33.9 °C 27 % RH
December 21st (03.21):	18.3 °C 33 % RH

The maximum humidity ratio (x_s) and absolute humidity (x) are established from the psychrometric chart according to the recorded climate data points identified above. The diffusion membrane evaporation rate is calculated for each season to provide the potential range for a 1.0 cm^2 surface area:

03.21: $g_h = 0.5(1)(19 - 1.9) = 8.55$ g/cm^2/hour

06.21: $g_h = 0.5(1)(38 - 8) = 15$ g/cm^2/hour

09.21: $g_h = 0.5(1)(35 - 9) = 13$ g/cm^2/hour

12.21: $g_h = 0.5(1)(14 - 4.5) = 4.75$ g/cm^2/hour

The hourly diffusion rate varies from approximately 4.75 g/cm^2/hour to upwards of 15 g/cm^2/hour. We utilize this information to develop the desired thickness and volumetric water holding capacity for the hydrogel membrane. The surface area and density (thickness) of hydrogel membrane is determined in conjunction with the evaporation rates required for effective downdraft cooling in Tucson's hot-arid climate.

2.1.1.2. Hydration and Saturation Rates

The rate of diffusion from the hydrogel membrane will inform the amount of water being used and the cycles for hydration that will be required. Initial saturation studies show that the 4% polyelectrolyte hydrogel will absorb water to full loading capacity at an average rate of approximately 60 g/cm^3/hour under hydrostatic conditions, though the actual rate of sorption varies following an isotherm curve.

Hydration cycles will be actuated through integrated sensing techniques. Dry-bulb, humidity, and photometric sensors will be located at select locations around the diffusion membrane, which is divided into four main segments. The sensors are linked to a control platform and algorithm that will indicate to one of four microfluidic pumps to initiate water-pumping to hydrate the membrane. The actuation of hydration is dependent in part on optical sensing of daylight transmission through the diffusion membrane (higher visible transmission indicates the membrane is saturated, while low visible transmission indicated more water may be needed). The other dependent condition for hydration actuation is the surrounding dry-bulb and relative humidity sensing, which indicates whether additional moisture is needed to enable the downdraft cooling process.

2.1.1.3. Volumetric Expansion and Contraction Kinetics

During the hydration and dehydration studies of the polyacrylamide hydrogel, measures for the respective swelling and deswelling kinetics were established. Maximum loading occurs when the hydrogel has reached full saturation capacity and is at its largest volumetric size. Dehydration to a completely dry state provides the minimum possible dimensions of the hydrogel. The dimensional change ratio is defined as the relation between the difference of these two states to the maximum loading.

The pilot test for deswelling kinetics demonstrates a dimensional change for three volumetric samples over a three-day period. The hydrogel exhibits an ability to modulate by 25% of its original dimensions and up to 50% of its original volume. The dimensional change is reversible. The modulation of both the weight and

dimensions inform the design for the membrane support framework, which requires a flexible mesh fabric to provide a composite hydrogel system (Fig. 2).

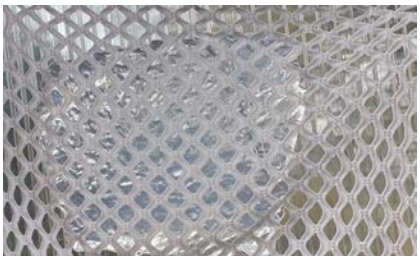

Figure 2. Hydrogel adhered to flexible mesh

2.1.2. Thermal Storage and Radiant Cooling

Thermal storage and radiant cooling phenomena are assessed for two different translucent materials. Physical material tests are conducted *in-situ* for the materials utilizing thermal sensing and thermography techniques.

2.1.2.1. Physical Material Testing

Material module pilot testing was conducted in Tucson on the rooftop of the building where the full-scale downdraft chimney prototype will be located. The pilot test data compares two heat capacitance and radiative cooling materials: Polyelectrolyte Hydrogel (PEG) and Phase Change Material (PCM) as shown in Figure 3. The PEG was synthesized at the Arizona Material Laboratories and is fully saturated with deionized water. The PCM is 100% paraffin with a 24°C melt point and was obtained from Microtek Laboratories.

Figure 3. Material pilot test setup: a) Polyelectrolyte Gel (PEG) and Phase Change Material (PCM) testing modules; b) FLIR camera used for thermography images; and c) Thermistor sensing for material temperature data collection

Each material module is encased in clear polyethylene and embedded with a thermistor to obtain 1-minute intervals for material temperatures. A rooftop weather station is also providing local micro-climate data for reference. The test-data was collected over a two-day period. The first day enables the heat-capacitance and radiative materials to normalize with outdoor weather conditions. The second day provides the baseline dataset. Initial test-data is provided for one testing period in summer season. Select intervals of IR-thermography are captured for the material modules during the testing timeframe.

Comprehensive thermal mass and radiative material testing is also currently underway and will be conducted for seasonal comparisons across an annual timeframe. The comprehensive testing matrix consists of nine configurations, each with four material modules (Fig. 4). Each configuration includes four clear polyethylene bags filled with different materials: water, polyacrylamide hydrogel, PCM, and one painted white with no filling. There is one configuration oriented at 180-degrees upwards for full sky-exposure reference. The other configurations are oriented at 90-degrees vertical and 45-degrees diagonal. Each cardinal orientation (North, East, South, and West) is documented concurrently during the testing in conjunction with microclimate data collected with the *in situ* weather station.

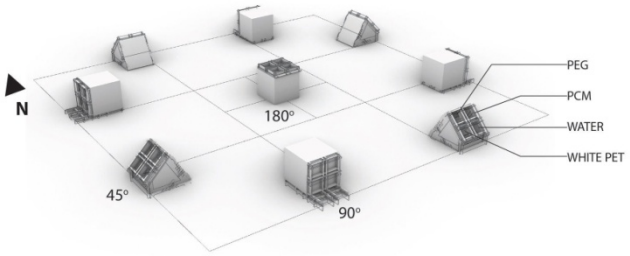

Figure 4. Diagram of the comprehensive heat capacitance and radiative material testing setup

2.2 Full Scale Prototype Simulations

The structure of the full scale prototype is currently under construction. Several simulations were conducted in order to optimize the self-shading of the chimney form and airflow into the building's interior.

2.2.1. Buoyancy Airflow from Evaporative Cooling

Analytical Model

The convective heat flow induced by evaporative cooling is first analyzed with a simplified analytical model used to determine the basic dimensions of the chimney and is then simulated by a CFD model in order to provide an understanding of the distribution of cooling and air under the chimney, i.e., inside of the building.

The free convection flow estimation can be summarized in Equations 2-5:

The difference between a target temperature (T_{in}) for the interior and outside air temperatures (T_{out}) during the day, together with the air's moisture content [7]. If we change the air's moisture content at the chimney's crown (assuming air as a constant pressure ideal gas), its density will increase by the following relationship:

$$\Delta\rho = \rho_{out} - \rho_{in} = \rho_{in} \times \frac{(T_{in} - T_{out})}{T_{out}} \quad (2)$$

where $\Delta\rho$ is the density difference between the ambient air and the cooled air; ρ_{out} and ρ_{in} are the densities of the air

outside and inside the chimney, respectively. The heat transfer (Q_{cv}) necessary to cool dry air by a specific temperature difference is given by:

$$Q_{cv} = \dot{v} \times C_{pa} \Delta T \quad (3)$$

where $\dot{v}$ is the volumetric flow rate per hour, defined by the number of people that occupy the cooled space; C_{pa} is the volumetric specific heat of dry air; $\Delta T$is the temperature gradient between the ambient and the cooled air.

The dense cooled air will drop down the chimney through free convection. We can find the cooled air's flow rate through:

$$Q_{flowrate} = V \times A \quad (4)$$

where A is the cross-sectional area of the chimney; $V$is the velocity of the air given by:

$$V = \sqrt{2gl \times \frac{\Delta\rho}{\rho_{out}}} \quad (5)$$

where g is the gravitational acceleration; l is the height of the chimney; $\Delta\rho$is the density difference between the ambient and the cooled air; ρ_{out} is the density of the air outside the chimney. The rate of water mass evaporated into the air from the hydrogel membrane surface was analyzed based on the diffusion rate described in section 2.1.1.1. At an average diffusion rate of g/cm^2/hour, it is sufficient for the air to be exposed to a quarter of the chimney's top funneled surface area, lined with the hydrogel membrane, (area of 9850 cm^2) for the air to cool down by 11^{o}C and drop at a velocity of 1.2m/s. This was the basis for the CFD simulation described in the next section. Additionally, the principle of the Coanda effect was maintained in regards to the surface curvature.

CFD Simulation Model

Computational Fluid Dynamic (CFD) studies were conducted with the Butterfly plug-in for Rhino-Grasshopper and the OpenFoam analysis engine. CFD analyses were used to determine the relationship between the chimney geometry and airflow speeds and morphologies into the space below. The parametric study addresses different heights and diameters of base, neck, and top zones of the chimney. Three iterations of chimney heights were evaluated, including 2-meters, 4-meters, and 6-meters. Three iterations of neck position were evaluated with locations at the midpoint, one-third from the top, and one-third from the base. The top, neck, and base diameters remain constant throughout the study.

The CFD simulation model is set up with the chimney located over the center of a square dimension space and depicts the inlet at the top of the chimney and one outlet at the wall of the space as shown in Figure 5. The analysis planes are established through the mid-sections of the space for plan and section views of the airflow results. The analysis grid was made with snappyHexMesh and blockMeshDict.

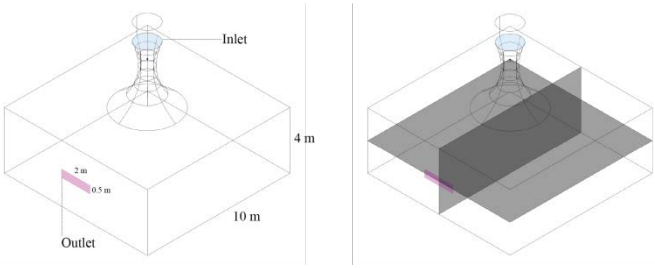

Figure 5. CFD simulation model setup depicting inlet at top of chimney and single outlet in space below (left) with two evaluation planes for plan and section analysis (right)

The current CFD analyses establish basic downdraft airflow patterns with an assumed inlet for downward airflow of θ=180^0 at a speed of 1.2 m/s from the top of the chimney. Future analyses will make use of local wind speeds and directions entering the top of the chimney from its side-apertures. The current analytical model for the CFD simulation is based on the finite volumetric method for simplification of understanding flow regime into the space below [22-23].

2.2.2. Radiative Heat Exchange

Solar Irradiation Analysis

In order to prevent overheating of the thermal mass by solar radiation gains, it is necessary to provide sun-shading to the material modules while still exposing them as much as possible to the cold sky. A series of radiation analysis simulations were conducted during the design development for the chimney framing system. The solar gain seasonal and diurnal radiation analyses were conducted with the Ladybug-Honeybee plugins for the Rhino-Grasshopper models [24]. The radiation analyses were informative in defining the depth of framing members to provide adequate shading during peak temperature conditions. The overall geometry of the chimney and orientation of framing members was also informed in part by the radiation studies. Ultimately, the radiation analysis for peak summer conditions defined the guide for locating appropriate material modules and establishing heat capacitance properties (i.e. thicknesses for hydrogel modules and melting temperatures for PCM modules). The results of solar irradiation on the chimney surface, in kWh/m^2 must be then multiplied by a reflectivity ratio of the material, to receive the heat gain of the actual thermal mass surface. Based on previous literature [5,6], we propose a shortwave reflective coating over the thermal mass membrane exposed to solar radiation, which is still emissive in the longwave to allow sky cooling. Thus, the solar heat gain can be reduced by about 90 percent.

Longwave Heat Loss to the Cold Sky

In order to estimate the radiative cooling impact of the sky, a simulation was conducted for test-points along the chimney's surface. Using the surface geometry modeled in Rhinoceros 3D modeling software, the simulation code was developed in Grasshopper algorithmic modeling. This

simulation technique was initially developed in the author's previous work [25] accounting for MRT per point in space. In this case, an array of equally spaced test points was placed on the surface of the chimney. For each point, the view factor of the sky and other surrounding surfaces was computed and the total radiation heat loss or gain from longwave radiation was calculated. Clear skies were assumed for this simulation, although cloudiness downwelling effect can be integrated based on TMY weather files. The clear sky temperature was assumed to vary between 1∘C to 12∘C based on sky temperature models by Berdahl and Fromberg [26] and Garg [27], for low dew point with clear sky. A continuous ambient air temperature is derived from TMY weather files. In the sample results shown here for one hour in the month of June, the air temperature was assumed to be 32∘C. The interior air temperature inside the chimney (and the interior face of the thermal mass) was assumed to be maintained at 27^{o}C due to the evaporative cooling downdraft airflow. Note that longwave radiation was accounted for from the sky and surrounding surfaces. The longwave portion of the solar radiation was included in the previous solar simulation and therefore not included in this simulation.

The results in kWh/m^2 are for a perfect blackbody emitter, while in reality, they must be multiplied by the emissivity coefficient of the surface material for the actual cooling potential.

3 RESULTS AND ANALYSIS

3.1 Material Testing Results

Results from the heat capacitance and radiative material tests are shown for the 24-hour cycle. The IR thermography images depict the fully loaded hydrogel and PCM modules at four-hour intervals from 9:30am on July 12th to 9:30am on July 13th (Fig. 6). The IR images were analyzed with the online FLIR software and assessed with two comparison zones per image: a) thermal mass material zone, and b) surrounding roof zone. The minimum and maximum IR surface temperatures for the material zone of the PEG are 7 ^{o}C at 5:30 AM and 61.3 ^{o}C at 1:30 PM respectively. The minimum and maximum IR surface temperatures for the material zone of the PCM are 6.4 ^{o}C at 5:30 AM and 60.9 ^{o}C at 1:30 PM respectively.

The thermistor sensing data was collected at 1-minute intervals for the 24-hour period and shows the material temperature fluctuations rising towards 60 oC by 2pm in the afternoon and dropping to minimum temperatures between 2am - 8am in the morning (Fig. 7). The minimum and maximum core temperatures for the PEG are 24.8 ^{o}C at 1:30 AM and 59.8 ^{o}C at 4:00 PM respectively. The minimum and maximum core temperatures for the PCM are 12. 6 ^{o}C at 6:15 AM and 60.1 ^{o}C at 1:45 PM respectively.

The PCM exhibits an ability to rapidly release more heat content in comparison with the hydrogel. Conversely, the hydrogel more rapidly increases its sensible heat as soon as it begins to receive direct solar radiation in the morning timeframe. It is important to note that if shortwave reflective coating is applied to the envelope of the thermal mass, the solar heat gain would be reduced significantly, while the sky cooling will be maintained. The separation of the thermal mass from direct ambient gain, as shown in [5], also contributes to its radiant cooling capacity.

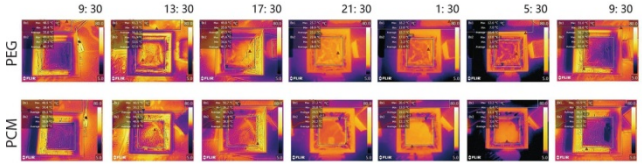

Figure 6. Infrared thermography images for PEG (top) and PCM (bottom) at four-hour intervals during pilot-test period July 12th-13th, 2019

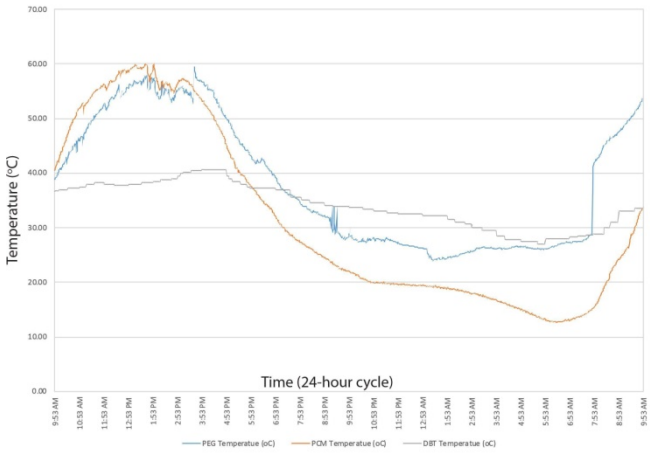

Figure 7. Material thermistor measures and dry-bulb temperature during pilot-test period July 12th-13th, 2019

3.2 Full-Scale Prototype Simulation Results

3.2.1. Airflow CFD results

The results of the parametric CFD simulations show that the tallest chimney height (6-meters) provides the greatest air velocity into the space below. Since the full-scale physical prototype will be constructed with a 4-meter height, the results for the 4-meter height chimney are shown for this study in Figure 8. The optimal neck position for the 4-meter height is located at the midpoint of the chimney to provide greater air speed for ventilation cooling effects throughout the space below. Since the number of outlets, outlet size, and outlet position also influence the airflow patterns and velocities, further studies will be conducted to evaluate optimal spatial choreography of the airflow.

The downdraft air speed maintains the highest velocity in the space directly below the chimney. Vortices form in the spaces of the room to the sides of the chimney aperture and follow natural convective buoyancy patterns. The air speed at the outlet increases in velocity due to the pressure differentials between outdoor and indoor conditions.

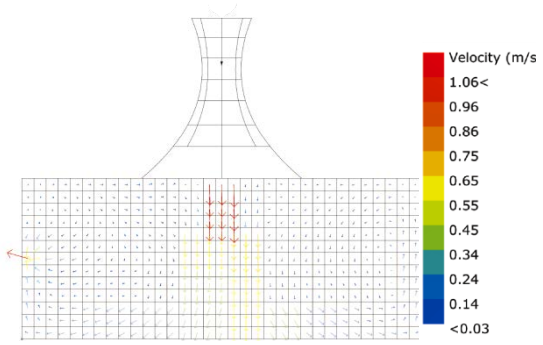

Figure 8. CFD results for optimal 4-meter height chimney

3.2.2. Radiative Heat Exchange Results

Solar Irradiation Analysis

The results show the radiative heat gain pattern of the chimney surface ranging between 0 kWh/m^2 for the fully shaded areas to 9 kWh/m^2 at the upper limit of solar heat gain per day, for completely unshaded areas (Fig. 9). For the actual material surface, assuming a shortwave-reflective coating, we can assume a multiplier of 0.1 for the results, reducing the heat gain significantly.

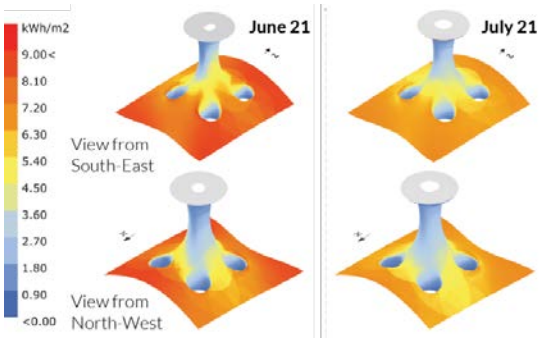

Figure 9. Solar irradiation simulation results for the chimney's surface for the duration of a full summer day of June and July 21st

Longwave Heat Loss to the Cold Sky

Figure 10 shows a sample result for one hour of longwave radiative heat exchange between the surface of the chimney and its surrounding in clear sky conditions in Tucson, Arizona in June. The results show heat gain rather than heat loss at the very top of the chimney due to the self-shading geometry preventing an exchange with the sky. The results also show heat gain at the bottom of the chimney, where its surface is in great proximity to the hot roof . The areas most advantageous for radiant sky cooling are in the middle portion of the chimney, and especially in the north and south portion as seen in Fig. 9. This is due to the surface slope in these portions of the chimney and its relationship to the overall geometry.

The results ranging between 0.0 and 0.09kWh/m^2 are for one hour of exposure only, unlike the radiation results which are for the full day. The heat loss will be greater at night and in the morning hours when the surrounding roof is cold and not contributing heat gain to the surface. The results should then be multiplied by the emissivity ratio of the thermal mass enclosure, which would reduce the total heat loss by about 10 percent.

If we compare the pattern from Figure 10 to the results from the solar irradiation analysis (Fig. 9), we can see that while the middle zone of the chimney is both well shaded from direct sun but still achieves heat loss at lower portion of the south and north segments that are the most advantageous for radiative cooling from the sky are also receiving large fluxes of solar heat gain during the day. For this reason, shortwave reflective coating should be applied to the modules placed in that portion to optimize heat loss and minimize heat gain. The combined results analysis are the guidelines by which the thermal mass will be placed on the final prototype and appropriate wavelength-specific coatings will be applied.

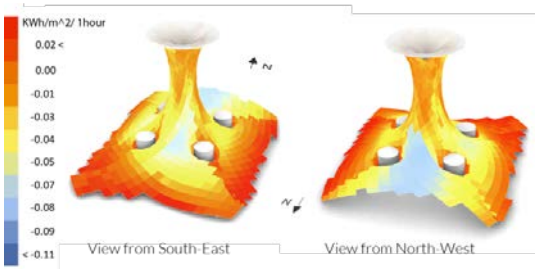

Figure 10. Longwave radiation heat loss/gain simulation results for one hour in the month of June with clear skies.

4 CONCLUSION AND FUTURE WORK

The various analytical, empirical, and simulation testing methods explored in this paper show the cooling potential for a combined radiative and evaporative cooling device in a desert climate. The analytical models for evaporative cooling through diffusion of moisture from the hydrogel membrane demonstrates the capacity of surface evaporation to create a buoyancy force sufficient to cool a significant volume below the chimney. Future CFD simulation models will combine the advanced characteristics of the chimney materials, including: a) moisture diffusion from the cooling membrane at the top (i.e. buoyancy model), and b) heat capacitance material temperature dynamics for the thermal mass modules of the chimney. The empirical test data for the material systems will be integrated into the CFD simulation model. The heat capacitance material tests and longwave radiation heat loss simulations show the combined ability for thermal lag and sky re-radiation to provide additional cooling and attenuate the heat peak during the day.

The next steps include the completion of the full-scale prototype currently under construction. The full-scale prototype will enable the collection of empirical data for downdraft cooling effects and air speeds at the space below the chimney. The empirical data can be compared with the ongoing development of the CFD simulation models. The radiant cooling capacity of the envelope will also be further explored through the full-scale prototype for validation of the simulation results.

REFERENCES

1. Givoni, B. (1993). Semiempirical model of a building with a passive evaporative cool tower. *Solar Energy*, *50*(5), 425-434.
2. Erell, E., Pearlmutter, D., & Etzion, Y. (2008). A multi-stage down-draft evaporative cool tower for semi-enclosed spaces: aerodynamic performance. *Solar Energy*, *82*(5), 420-429.
3. Altman, T., Zaslavsky, D., Guetta, R., & Czisch, G. (2005). Evaluation of the potential of electricity and desalinated water supply by using technology of" Energy Towers" for Australia and America. *Interim Report.*
4. Craig, S., Harrison, D., Cripps, A., & Knott, D. (2008). BioTRIZ suggests radiative cooling of buildings can be done passively by changing the structure of roof insulation to let longwave infrared pass. *Journal of Bionic Engineering*, *5*(1), 55-66.
5. Raman, A. P., Anoma, M. A., Zhu, L., Rephaeli, E., & Fan, S. (2014). Passive radiative cooling below ambient air temperature under direct sunlight. *Nature*, *515*(7528), 540-544.
6. Goldstein, E. A., Raman, A. P., & Fan, S. (2017). Sub-ambient non-evaporative fluid cooling with the sky. *Nature Energy*, *2*(9), 1-7.
7. Aviv, D., & Meggers, F. (2017). Cooling oculus for desert climate–dynamic structure for evaporative downdraft and night sky cooling. *Energy Procedia*, *122*, 1123-1128.
8. Aviv, D., & Kilian, A. (2018). Climate-Adaptive Volume: Solving the Motion Envelope of a Reconfigurable Cooling Aperture for Desert Climate. *Technology| Architecture+ Design*, *2*(2), 186-195.
9. Charoudi, D. U.S. Patent No. 3 953 110 (27 April 1976).
10. Designbloom. “IAAC students create hydroceramic: a passive cooling system for buildings.” *designbloom*. (2014). Retrieved from https://www.designboom.com/architecture/iaac-dmic-hydroceramic-passive-cooling-system-09-18-2014/
11. Smith, S. I. (2017). Superporous Intelligent Hydrogels for Environmentally Adaptive Building Skins. *MRS Advances*, *2*(46), 2481-2488.
12. Moradnejad, M., Aviv, D., Ida, A., & Meggers, F. (2019). WATeRVASE: Wind-catching Adaptive Technology for a Roof-integrated Ventilation Aperture System and Evaporative-cooling. *Building Technology Educator's Society*, *2019*(1), 50.
13. Fornasiero, F., Tang, D., Boushehri, A., Prausnitz, J., & Radke, C. J. (2008). Water diffusion through hydrogel membranes: A novel evaporation cell free of external mass-transfer resistance. *Journal of Membrane Science*, *320*(1-2), 423-430.
14. P. M., V., Bayraktar, O., and Picó, G. *Polyelectrolytes Thermodynamics and Rheology (Engineering materials)*. (2014). New York, NY: SpringerLink.
15. Huang, C., Dostalek, J., and Knoll, W. “Long range surface plasmon and hydrogel optical waveguide field-enhanced fluorescence biosensor with 3D hydrogel binding matrix: On the role of diffusion mass transfer.” *Biosensors & Bioelectronics, 26(4)*, (2010): 1425-31.
16. Bhattacharyya, D., Schäfer, T., Wickramasinghe, S. R., & Daunert, S. (Eds.). (2013). *Responsive membranes and materials*. Chichester: Wiley.
17. Flory, P.J. and Rehner, J. “Statistical Mechanics of Cross-Linked Polymer Networks: II. Swelling.” *Journal of Chemical Physics, 11* (1943): 521-526.
18. Richter, F. “Timescales determining the degree of kinetic isotope fractionation by evaporation and condensation.” *Geochimica Et Cosmochimica Acta, 68(23)*, (2004): 4971-4992.
19. Jirka, G. H., & Brutsaert, W. (1984). Measurements of wind effects on water-side controlled gas exchange in riverine systems. In *Gas Transfer at Water Surfaces* (pp. 437-446). Springer, Dordrecht.
20. Bellucci, M., and Trout. "Note: On the Evaporation Coefficient of Water." *The Journal of Chemical Physics, 21* (2014): Vol.140(15).
21. Eames, I.W, Marr, N.J and Sabir, H. "The Evaporation Coefficient of Water: A Review." *International Journal of Heat and Mass Transfer, 40.12* (1997): 2963-973.
22. Welahetti, P., & Vågsæther, K. (2016). Comparison of OpenFoam and ANSYS Fluent. Computational Fluid Dynamic Simulation of Gas-Gas Single Phase Mixing with and without Static Mixer.
23. Hedayat, Z. H., Samkhaniani, N., Belmans, B., Ayatollahi, H., Wouters, I., & Descamps, F. (2015, December). Energy modeling and air flow simulation of an ancient wind catcher in Yazd. In *3rd International Congress on Civil Engineering, Architecture and Urban Development* (pp. 29-31).
24. Roudsari, M. S., Pak, M., & Smith, A. (2013, August). Ladybug: a parametric environmental plugin for grasshopper to help designers create an environmentally-conscious design. In *Proceedings of the 13th international IBPSA conference held in Lyon, France Aug*.
25. Aviv, D., E. Teitelbaum, T. Kvochick, K. Bradford, and Forrest Meggers.(2019). Generation and Simulation of Indoor Thermal Gradients: MRT for Asymmetric Radiant Heat Fluxes. In *Proceedings of Building Simulation*. Rome, Italy: IBPSA.
26. Berdahl, P., & Fromberg, R. (1982). The thermal radiance of clear skies. *Solar energy*, *29*(4), 299-314.
27. Garg, H. P. (1982). *Treatise on solar energy*. John Wiley & Sons.